Spectral tuning and signaling of diverse and most red sensitive visual rhodopsins that drive high colour discrimination in Mantis Shrimp eyes

Camille Brouillon[1]*, Alina Pushkarev[1]*†, Marjorie A. Liénard[2]*†, Songhwan Hwang[1,3],Arno Munhoven[1], Richard McDowell[4], Robert J. Lucas[4], Megan Porter[5], Han Sun[3,6], and Peter Hegemann[1]†

[1] Institut für Biologie, Experimentelle Biophysik, Humboldt-Universität zu Berlin, Invalidenstr. 42, D-10115 Berlin, Germany
[2] GIGA Institute, University of Liège, Avenue de l'hôpital 11, 4000 Liège, Belgium
[3] Leibniz-Forschungsinstitut fu r Molekulare Pharmakologie, Berlin 13125, Germany
[4] Centre for Biological Timing, Department of Neuroscience, University of Manchester, Oxford Road, Manchester, M13 9PT, United Kingdom
[5] School of Life Sciences, University of Hawai'i at Mānoa, Honolulu, HI 96822, USA
[6] Institute of Chemistry, Technische Universität Berlin, Berlin 10623, Germany

† Correspondence: Alina Pushkarev (alinadrusilla@gmail.com); Marjorie A. Liénard (marjorie.lienard@uliege.be), Peter Hegemann (hegemann@rz.hu-berlin.de)

* These authors contributed equally to this work.

Keywords: Retinal proteins, Bistable rhodopsins, GPCR, Membrane receptors, G-signaling, Crustacean vision, Sensory systems

Abstract

Of all visual systems shaped over billions of years, stomatopod crustaceans or mantis shrimps possess arguably one of the most extraordinary eyes, with unmatched potential for broad colour detection [1–3]. Yet how their unusual diversity of visual opsins [4] maps onto functional spectral sensitivities [5,6] has remained unresolved. Here, we uncover the molecular rhodopsin-based physiological mechanisms of spectral tuning and show that seventeen opsins, mostly from the colour-sensing midband of the *Neogonodactylus oerstedii* eye, exhibit distinct spectral absorption ranges and couple to Gq- or Gi-proteins. Two mid-wavelength opsins (NOMs) preferentially absorb blue light, while twelve long-wavelength opsins (NOLs) absorb in the green range. In addition, three NOLs are red-sensitive beyond 600 nm, representing the most far-red-sensitive opsins functionally characterized in animals. Several opsins exhibit photoreversibility with inverse blue-red spectral shifts, revealing an unrecognised layer of photochemical flexibility in stomatopod photoreception. Combined with ommatidial carotenoid filters, our mechanistic model shows how individually tuned rhodopsins shape row-specific spectral sensitivity across the eye, promoting far-red sensitivity in tier 3P in relation to other spectral wavelengths. These specialised rhodopsin-filter combinations collectively enable robust colour vision along a broad light spectrum and across dim and bright conditions, offering new insights into the evolution of one of Nature's most sophisticated visual systems.

Mantis shrimps are stomatopod crustaceans that possess one of the most unusual and sophisticated visual systems among all known animals. The Caribbean species *Neogonodactylus oerstedii* (Fig. 1a) inhabits shallow-depth marine waters bathed with a broad spectrum of light, and its prominent highly mobile eyes bear at least 12 photoreceptor classes each tuned to specific wavelength ranges between 300 nm to 700 nm, a remarkably high number unmatched thus far in animals, and whose role in colour vision has long intrigued the scientific world [6]. Photoreceptor diversity arises through three distinct regions, the dorsal and ventral hemispheres devoted to spatial and motion vision, and six central rows of ommatidia (the midband or MB) that run along the equator of the eye (Fig. 1b), with rows 1-4 mediating color discrimination [7], whereas rows 5-6 are responsible for polarization vision [3]. In rows 1-4, three stacked tiers of cells act as successive filtering layers, absorbing a portion of the light spectrum available to cells below. In rows 2 and 3, carotenoid-packed vesicles interspersed between the distal and proximal photoreceptive layers [8] considerably tune the light available to their underlying photoreceptors.

In a seminal publication, Cronin and Marshall [1] measured bleaching spectra from *N. oerstedii* retinal ommatidial cross-sections for all of the anatomically distinct photoreceptors absorbing within the visible spectrum. These spectra revealed absorbance maxima between 401 and 551 nm, presumed to correspond to one dominant rhodopsin (opsin with retinal chromophore) in each tier, under the assumption that all cells within a given tier expressed only a single one. The absorption spectra of the intra-rhabdomal coloured filter pigments were also measured to estimate the resulting sensitivities of midband receptors [1]. These filters showed strong spectral

overlap with their underlying photoreceptor sensitivity, an overlap that was expected to dramatically reduce photon capture by up to more than three orders of magnitude (>1000-fold) in the proximal tier 3P, thereby proposed to confer red-light selectivity in 3P, but with very low overall sensitivity, an adaptation potentially useful for the animal under bright light conditions [9]. Wavelength dependent intracellular electrophysiological recordings (E-phys) of the UV-sensitive R8 cells in *N. oerstedii* [2], later complemented by measurements spanning 400 and 700 nm for a number of related shallow-and deep-water stomatopods [6,10], support that together the UV-sensitive R8 cells and the separated R1-7 tiers of ommatidial rows 1-4 in *N. oerstedii*, enable multi-chromatic sampling across the UV-visible spectrum, and spectral processing via colour-opponency and wavelength binning-mechanisms [5,11].

Early physiological evidence further suggested that the mantis shrimp eye can sense far red light and led to the proposal that red-sensitive cells in row 3 result from strong intra-rhabdomal filtering of a presumably limited opsin set [3,12,13], similarly to most invertebrate organisms [14]. However, although less sensitive photoreceptors would be expected compared to other midband rows, E-phys sensitivity was remarkably similar between the red-sensitive photoreceptors in row 3 and other photoreceptor types [3,12], leaving unresolved the molecular mechanisms underlying far red sensitivity.

Most animal visual pigments absorb maximally in the visible range (λ_{max} 400-580 nm), and many taxa also have receptors sensitive to ultraviolet wavelengths (<400 nm) [15], but efficient red light-absorbing rhodopsins are remarkably rare in animals. So-called red-sensitive opsins generally maximally absorb around 560-580 nm when using an 11-*cis* A1-retinal chromophore and only the far end of the opsin absorbance spectrum

reaches into the red part of the light spectrum [16–21]. Extreme red sensitivity (>600 nm) is typically achieved either by coupling a long-wavelength sensitive (LWS) opsin to a

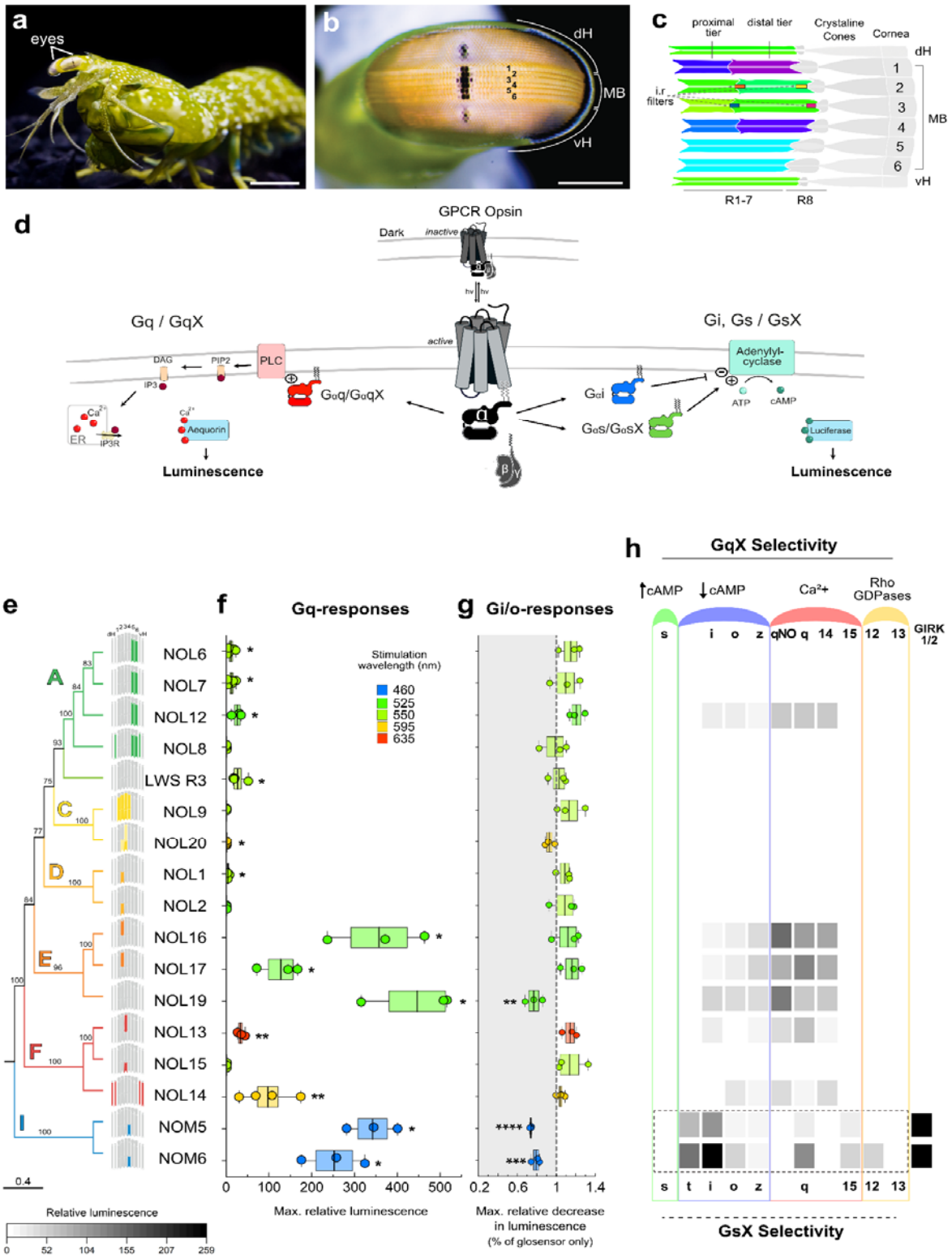

Figure 1. G-protein signaling properties of *Neogonodactylus oerstedii* rhodopsins in HEK cells

a. Photograph of a *N. oerstedii* mantis shrimp (scale bar = 5 mm). **b**. Close view of the external division of the compound eye composed of 6 midband rows (MB), and dorsal (dH) and ventral hemispheres (vH) (scale bar = 1mm) (from Porter et al. (2020) with permission). **c** Sagittal cross section diagram of the internal organisation of the retina, including intra-rhabdomal filters (i.r. filters), *i.e.* sitting within the rhabdom itself. Midband photoreceptive units 1-6 are colorized to match maximal photoreceptor absorbance as measured by microspectrophotometry and subdivided by tiers in rows 1-4 [34]. **d.** Scheme of bioluminescent second messenger assays with G□q signalling via PLC and G□s/G□i stimulating or inhibiting adenylyl cyclase (See methods for more details). **e.** Localization patterns (scale bar = 200 µm) and evolutionary relationships from Porter et al. 2020. **f**. Summary of maximal relative aequorin Gq-responses and **g.** glosensorGi/o responses (see Suppl. Fig. S2), presented as mean ± SEM, compared to cells transfected only with luminescent reporters. Significant responses are marked with (*). **h.** GqX- and GsX-protein coupling profiles of NOMs and NOLs.

retinylidene chromophore with an extra double bond (11-*cis* A2-retinal) [22–26], by addition of a bacteriochlorophyll light harvesting chromophore [27], or in combination with filters, such as oil droplets in birds, and carotenoid pigments in insects and crustaceans [9,28,29].

A key missing piece of the puzzle is how these properties build upon the unique opsin diversity recently uncovered in the eye of *N.oerstedii*, with 33 RNA-transcripts grouped into 17 distinct expression patterns and frequent co-expression across phylogenetic spectral clades [4]. We sought to uncover how multiple specialized rhodopsins and the distribution of carotenoid pigments interact to tune colour discrimination abilities in the Mantis shrimp eye. Specifically, we set up to test whether undiscovered rhodopsins are more efficient in detecting very long-wavelengths of light to extend sensitivity into the far red.

Three long-wavelength rhodopsins drive absorbance to the far red

To test this hypothesis while eliminating the influence of co-expressed visual pigments and filter components, we set out to fully characterize the remarkable opsin diversity *in vitro* outside the tremendous complexity of the native eye. First, we reanalyzed the genetic diversity and phylogenetic relationships (Fig. S1) of long- (NOLs), and middle- (NOMs) wavelength sensitive opsin clades depending on the amino acid signature of the predicted protein retinal binding pocket. We selected and heterologously expressed the 17 opsins mostly found across the eye hemispheres and midband rows 1-4 used for colour discrimination, comprising 15 full-length NOLs, and 2 NOMs of row 4 (Extended Data Fig. 1, Fig. S2) [4,30]. After reconstitution with the A1 11-*cis*-retinal chromophore used in crustaceans and most other invertebrates [31–33], the NOM5 and NOM6 opsins absorbed maximally at 455 nm and 459 nm in line with microspectrophotometric (MSP) data [34] and their phylogenetic placement in middle wavelength sensitive clades (Fig. S1, Extended Data Figs. 1,2). 12 NOL rhodopsins spanning phylogenetic clades A,C,D,E and F [4], exhibited absorbance spectra with maxima near 540 nm (Extended Data Fig. 2). Interestingly, NOL13 and NOL14 (clade F) as well as NOL20 (clade C) formed long-wavelength sensitive rhodopsins reliably absorbing maximally near and above 600 nm (Extended Data Fig. 2). These spectra appeared considerably red-shifted compared to predictions from averaged ommatidial bleaching spectra resulting from MSP recordings on *N. oerstedii* eyes [1], illustrating unique novel rhodopsin spectral sensitivities, potentially less expressed or whose contributions might have been previously overshadowed in the eye.

Long-wavelength opsins couple mostly to Gq and middle-wavelengths to Gi and Gq.

We next wondered if the *N. oerstedii* functional opsins were actively involved in the phototransduction cascade. We tested G-protein coupling and selective signaling preferences in each opsin using bioluminescent second messenger assays in HEK293T cells. To first test individual rhodopsins coupling to each of the three main families of human G-proteins, we tested the relative activation of Gq, Gi/o and Gs [35] (Fig. 1d,e, Extended Data Fig. 2). Five NOL rhodopsins (2, 8, 9, 15 and 20) did not elicit measurable responses to any G-protein type compared with cells transfected only with aequorin or glosensor, despite robust protein expression levels at the plasma membrane (Fig. S2), suggesting that they do not couple to human G-proteins. Ten NOL rhodopsins (1, 6, 7, 12, 13, 14, 16, 17, 19, 20), LWSR3, as well as NOM5 and NOM6 coupled significantly to Gq ($p<0.04$, Fig. 1e, Extended Data Fig. 3, Table S1), although signal intensity between rhodopsins may not be directly comparable, notably owing to different expression levels, membrane targeting, and G-protein coupling efficiencies. We could not detect activation of Gi or Gs for any NOL rhodopsin except for NOL19, however NOM5 and NOM6 reacted readily with Gi ($p< 0.001$, Fig. 1e, Extended Data Fig. 3, Table S1).

We further investigated the G-protein selectivity profiles by co-expressing *N. oerstedii* opsins in HEK293 cells that lack endogenous G-proteins [36], with individual human GsX chimeric proteins where the rhodopsin-interacting helix had been exchanged for helices of other G-subtypes [37]. Again, NOM5 and NOM6 both exhibited higher G-protein coupling to Gsi than to Gst, whereas NOM5 had lower responses to

GsX chimeras of the Gq family compared to NOM6 (Fig. 1f, Extended Data Fig. 3). As most of the signaling NOLs did not couple efficiently to GsX proteins but demonstrated significant Gq-responses, human GqX hybrids [38,39] were used following the same principle of the GsX assay (Fig. 1f). The Gq signal was quantifiable with enough variability to allow a reliable discrimination between GqX responses from six NOLs (NOL12, 13, 14, 16, 17 and 19) (Fig. 1f). All six characterised NOLs exhibited higher selectivity to GqX proteins of the Gq family, i.e. Gq or Gq14, but not Gq15 (Fig. 1f, Extended Data Fig. 3). In addition, all six NOLs showed weaker coupling to the Gi/o family of GqX proteins, with NOL14 in particular exhibiting comparatively high coupling to Gqo (21.9% of the sum of the GqX-protein selectivity responses, Extended Data Fig. 3). None coupled significantly to GqX components of the G12/13 or Gs families. In particular, NOL13 activated preferentially in presence of Gq (43%) and Gqi (9.6%), and significantly less with Gqz and Gqo (Fig. 1f, Extended Data Fig. 3). We also tested the only so far reported native *N.oerstedii* Gq-protein (GqNO) putatively involved in phototransduction [30] and found that all six NOL Gq-rhodopsins also activate Mantis Shrimp GqNO (Fig. 1f) but not with better signaling than for human Gq, except for NOL16 and NOL19 (both 37% to GqNO and 17% to Gq, Extended Data Fig. 3d-e). Overall, not including that some unresponsive NOLs may couple to other potential native GqNO-proteins, these results identify at least 13 functional opsins actively coupling to G-proteins thereby parsimoniously contributing to phototransduction in the mantis shrimp eye.

Rhodopsin action spectra and photoreversibility

Due to the strong Gq responses, we measured the wavelength dependence of Gq activation for NOL12, NOL16, NOL17 and NOL19, four green-sensitive opsins expressed across rows 2, 5 and 6. We constructed individual action spectra that closely resembled the *in vivo* rhodopsin absorption profiles [1,40,41] (Extended Data Fig. 2), overall aligning both approaches to confirm these four rhodopsins' green-sensitivity.

Owing to its shallow water habitat and visual ecology, *N. oerstedii* is subject to fluctuating light and colour distribution, which encouraged us to study the signalling specificity. To examine this question experimentally, we leveraged our Gq assay with the eight most promising, Gq-active rhodopsins (6 NOLs, 2 NOMs), and implemented double pulse experiments to examine their photoreversibility properties, by delivering a first pulse of light for Gq activation, and a second pulse for deactivation, and quantifying rhodopsin conversion back to their original D-state (Fig. 2a) [42,43].

Wavelength-dependent activation and deactivation spectra recorded for aequorin luminescent responses of NOM5, NOM6, NOL13, and NOL14 are presented in Fig. 2b,c. We first activated NOM5 and NOM6 with a 1s-light pulse of fixed wavelength at near-saturating light intensity (450 nm) and tested their Gq responses after a second red-shifted 1s-light pulse of varying wavelengths. We found a maximal reduction of 28.1% of the initial response at 583 nm for NOM5 and 21.58% at 580 nm for NOM6 (Fig. 2c). Plotting the inverse of this reduction against wavelength reveals the active Meta (L-) state spectra of the NOM photopigments which are photoreverted to the dark

(D-) state with the second light pulse (Fig. 2c). The dark activation spectra presented a dual spectral composition that was best fitted with a two-component Gaussian Model,

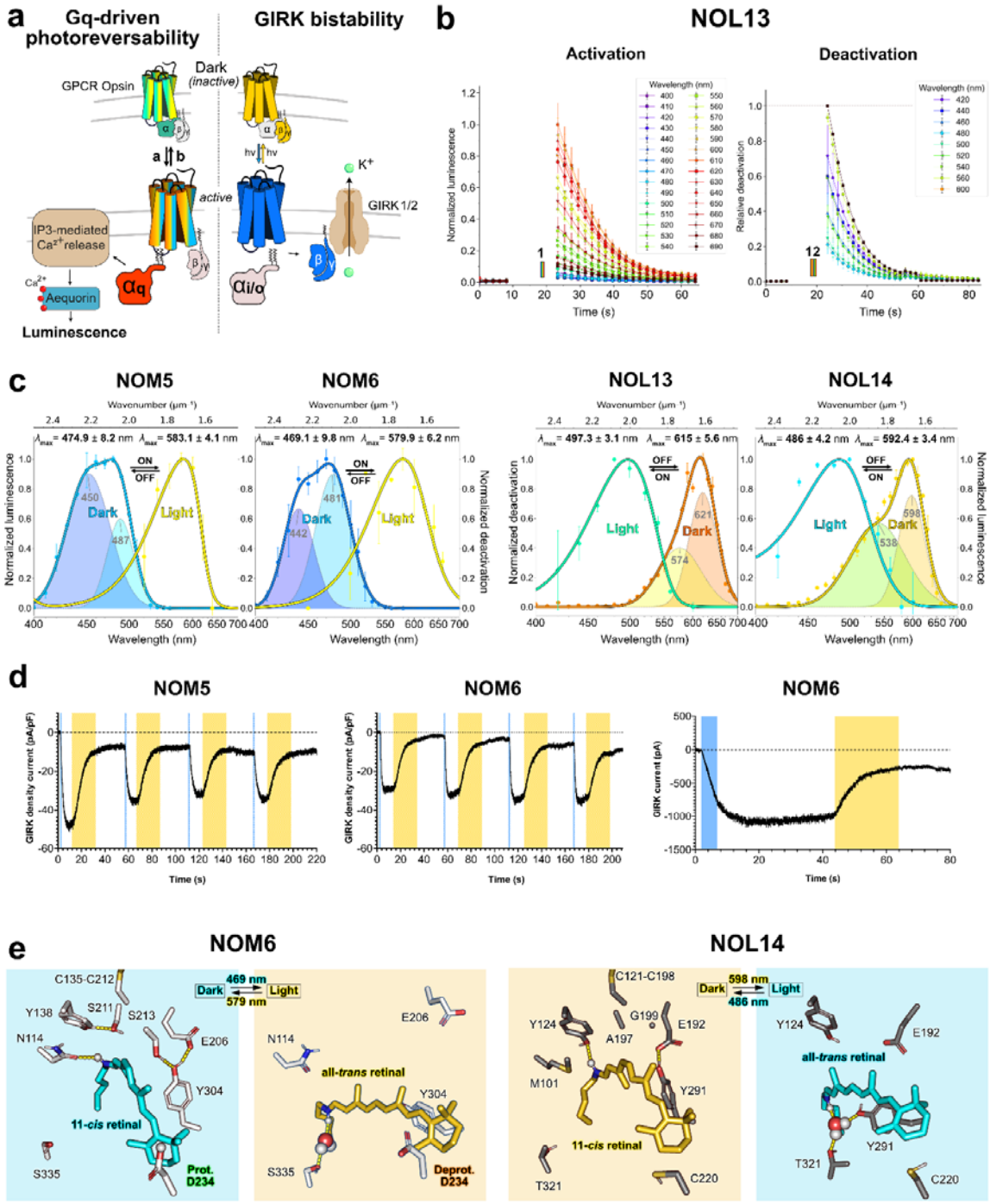

Fig. 2. Photoreversible *N.oerstedii* rhodopsins have opposite spectral properties explained by distinct retinal schiff base microenvironments

a. Activation and deactivation of the Gq pathway (*left*) and the GIRK1/2 channel (*right*) by a Gq- and Gi/o-coupled GPCR opsin, respectively. **b.** Wavelength-dependent aequorin luminescent activation/deactivation responses of NOL13. See SI for other Gq-activated rhodopsins. (*left*) Activation is induced by a 1s light pulse (colored rectangle 1) of fixed wavelengths at every 10 nm from 400 to 690 nm at $1x10^{16}$ photons cm^{-2} s^{-1} (n=3 experiments). (*right*) Deactivation is assayed by two consecutive 1s light pulses, one with the fixed wavelength leading to maximal activation (orange rectangle 1, 600 nm, $1x10^{16}$ photons cm^{-2} s^{-1}) followed by a second light pulse of varying wavelength with 15nm bandwidth (colored rectangle 2, $1x10^{16}$ photons cm^{-2} s^{-1}, n=3). **c.** Activation and deactivation spectra of NOM5, NOM6, NOL13 and NOL14, derived from peak aequorin responses and fitted with a non-linear least squares optimization of the Govardovskii visual template . Dark spectra are fitted with a two component Gaussian Mixture Model (GMM) (Table S1 and Fig. S3) Data is presented as mean values ±□SEM. X-axis is a linear energy scale (μm^{-1}) corresponding to a log wavelength scale (nm). **d.** GIRK photocurrents induced by the activation of NOM5 and NOM6 (1s blue light pulse, blue line) and deactivated by a subsequent 20s light pulse (yellow bar). Example of a stable NOM6-mediated GIRK current (*right*) evoked by a 5s 470 nm activation pulse of $1x10^{14}$ photons cm^{-2} s^{-1} and a 20s deactivation 595 nm pulse of $4x10^{15}$ photons cm^{-2} s^{-1}), respectively. **e.** Predicted structural models of the inactive NOM6 and NOL14 with 11-*cis* Retinal Schiff Base (RSB) and active (all-*trans* RSB bound) states of NOM6 and NOL14. Key hydrogen-bonding interactions are shown as yellow dashed lines and water molecules are represented as spheres.

suggesting a potentially pH-dependent heterogeneity of the protein (Fig. 2c, Table S2, Fig. S3).

Similarly, NOL13 and NOL14 activation responses were acquired with a 1s-pulse fixed at 600 nm, and thereafter their Gq-response reduction was quantified after blue-shifting the second light pulse, leading to maximal deactivation (75.1%) at 497 nm for NOL13, and reduced NOL14 response up to 55.7% at 486 nm. Visual fitting characteristics of the dark state also indicated the contribution of two spectral isoforms (Fig. 2c, Fig. S3). In contrast, for NOL12, 16, 17 and 19, no second light pulse could change the response to the first, suggesting that these rhodopsins are not photoreversible or have closely overlapping spectra in the dark and photo-activated states.

Finally, bistability and kinetic properties of NOM5 and NOM6 were further investigated electrically using the well established G protein-gated inwardly-rectifying potassium channel GIRK1/2 which canonically activates upon binding of the Gβγ

subunit of Gi/o-proteins [44] (Fig. 2a). Importantly, the Gi-responsive NOM5 and NOM6 could repetitively activate and deactivate GIRK1/2, with blue and orange light respectively, and with a limited loss in current amplitude, confirming that these opsins are thermally photoreversible and bistable (Fig. 2d). Of note, even after using a 20 second pulse for deactivation at maximal light intensity (20s, $4x10^{15}$ photons cm^{-2} s^{-1}), GIRK photocurrents could never completely recover to the pre-illumination baseline, likely due to the still overlapping dark and photoproduct spectra at the absorbance tails and the high light intensity required to revert the opsins to the dark state. Nevertheless, the photoproduct spectra of all four rhodopsins, which are considered as signalling states, were well separated from the dark state spectra (Fig. 2c). GIRK currents indicated kinetics of light-induced activation-deactivation responses and the thermal stability of the signaling state for NOM5 and NOM6 (Fig. 2d).

Thus, NOM5, NOM6, NOL13 and NOL14 are not only stable after photoexcitation without bleaching, they are also capable of returning to their inactive dark state photochemically due to the weak overlap of the D- and L-spectra.

Inverse spectral tuning of NOM6 and NOL14 arises from distinct retinal binding pocket properties

To gain a better understanding of the pronounced spectral differences between the dark states (D) and photoproducts (L), as well as the inverted photochemical shifts observed between NOM6 and NOL14, we generated structural models of the retinal binding pockets while maintaining the retinylidene chromophore protonated (Fig. 2e, Extended Fig. 4). The structural transitions from 11-*cis* retinal in the D-state to all-*trans* retinal in the L-state were modeled by combining AlphaFold3 predictions with multiple sequence

alignment (MSA) manipulation [45,46], molecular docking, all-atom molecular dynamics (MD), hybrid quantum mechanics / molecular mechanics (QM/MM) simulations, and vertical excitation energy calculations.

The predicted 7TM helix structure models exhibit high overall confidence, with predicted local distance difference test (pLDDT) values mostly above 80, and high structural stability during equilibrium MD simulations (Extended data Fig. 4, Figs S4-5). The counterions E206 and E192 are positioned unusually distant from the retinal in both proteins, only NOM6 features a unique acidic residue (D234) near the β-ionone, which is replaced by a cysteine (C220) in NOL14.

Comparison of the predicted absorption spectra for different protonation states of D234 in NOM6 revealed that a protonated D-state and a deprotonated L-state showed the closest agreement with the experimental data (Fig. S6) in consistency with the original double-point charge model proposed for rhodopsins [47,48], in which a negative charge near the β-ionone electrostatically stabilises the positive charge that formed in this region upon retinal photoexcitation causing a strong red shift. Next, we sought to rationalise the inverse spectral shifts observed between NOM6 and NOL14 by comparing their QM-optimized structural models. Notably, in NOM6 the residues flanking the disulfide bond are polar (S211 and S213) and S211 forms a hydrogen bond with Y138, while S213 interacts with Y304 and indirectly the counterion E206. The S211-Y138 interaction redirects the N-H of the retinal to N114 increasing polarity at the retinal nitrogen (Fig. S7). In contrast, in NOL14, the disulfide neighbors are nonpolar (A197 and G199). And the *11-cis* retinal N-H occasionally binds with Y124, while Y291 interacts with the counterion E192 only. The resulting reduced retinal distortion results

in greater π-conjugation and a red shift, compared to the distorted C12-C15 bonds in NOM6 (Fig. S8). The all-*trans* retinylidene N-H group in NOL14 forms a water-mediated hydrogen bond with T321, and occasionally to Y291. This configuration electrostatically stabilizes the ground state, increasing the excitation energy and causing a blue shift while the deprotonated D234 near the ring in NOM6 exerts the opposite effect, inducing a red shift. In conclusion, we propose that the inverse spectral shifts observed between NOM6 and NOL14 arise from substantial differences in the polarity and hydrogen-bonding networks within their retinal binding pockets. Such variations modulate the extent of π-conjugation and geometric distortion of the retinal, thereby fine-tuning its absorption characteristics.

Modeling the tuning of rhodopsin sensitivity with and without filtering pigments partitions photoreceptor spectral specialization

Next, we investigated how the multiple rhodopsins of the eye hemispheres, and midband ommatidial tiers tune photosensitivity without or under the influence of inter-rhabdomal filtering pigments, respectively. In the lateral dorsal and ventral hemispheres (DH and VH) devoid of inter-rhabdomal filtering, NOL14 with λ_{max} = 592 nm is expressed in conjunction with NOL8 with λ_{max} = 540 nm. Together they confer an unfiltered broad sensitivity (Extended Data Fig. 5) which is at least half maximal between 470 to 660 nm. This offers the dorsal and ventral sides of the mantis shrimp eye an exceptional ability to perceive from blue to very long-wavelength incoming terrestrial red light, the latter possibly persisting at very shallow depths, especially at dusk and dawn [49,12].

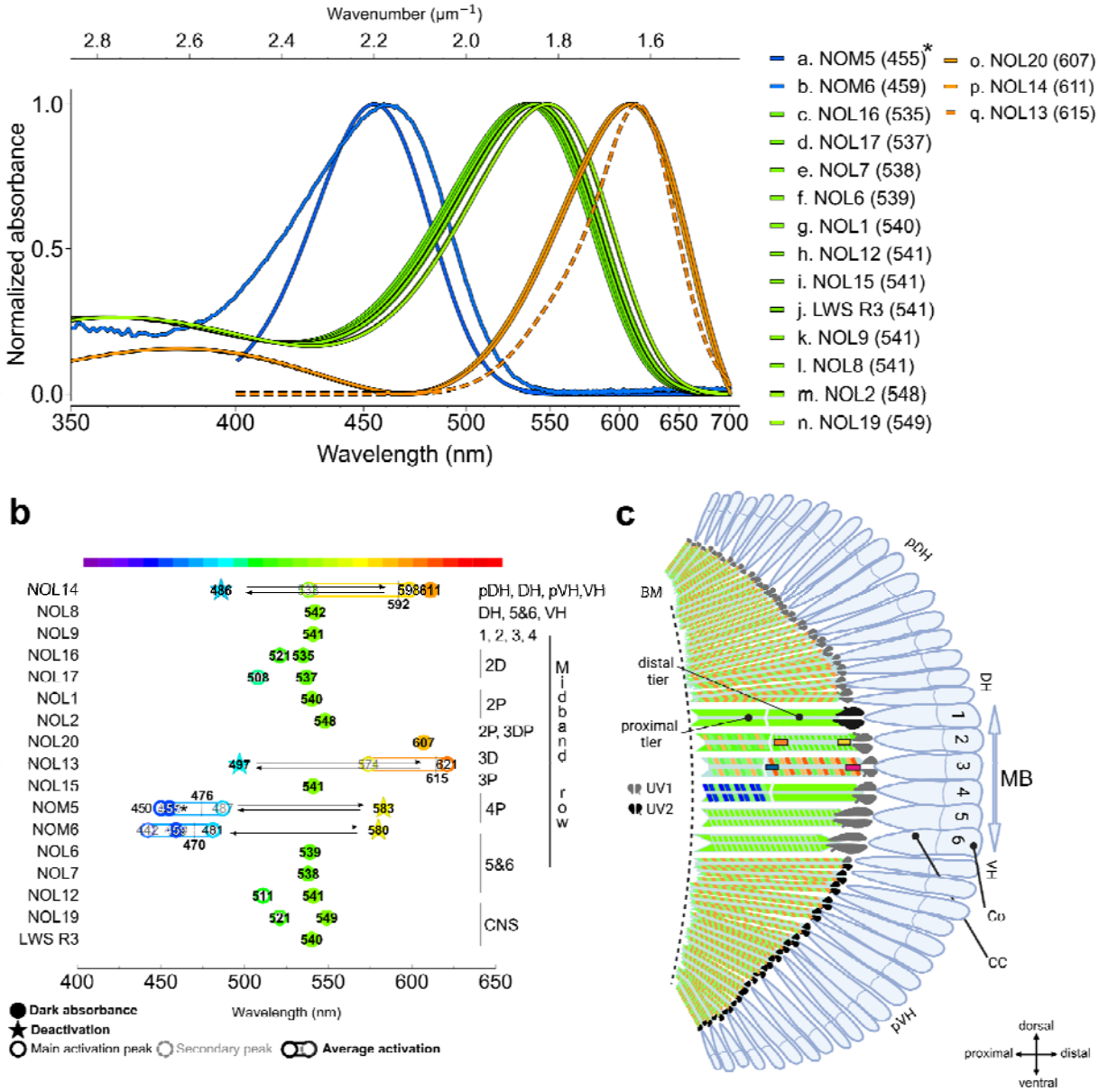

Figure 3. Multiple specialized spectral and photoreversible rhodopsins contribute to sharp, finely-tuned photoreceptor properties in the mantis shrimp retina

a. Spectral fits of dark NOL and NOMs absorption with 11-*cis* retinal or 9-*cis* retinal (*) full lines. For NOL13 the action spectrum is plotted in a dashed line (see Extended Fig. 2, Fig. 2). X-axis is a linear energy scale (μm^{-1}) corresponding to a log wavelength scale (nm) **b.** Absorbance maxima of mid- and long-wavelength rhodopsins characterised in this study, arranged by localization in different regions including eye hemispheres, eye midband rows 1 to 6, or the central nervous system (CNS). DH, dorsal hemisphere; VH, ventral hemisphere; p, peripheral; D, distal tier; P, proximal tier. Numbers indicate best-fit estimates of λ_{max} as measured with *11-cis* retinal (or *9-cis* retinal (*)) from dark absorbance (full circles), plus activation (empty circles), and deactivation spectra (stars) when measurable. Maximal activation for NOL13, NOL14, NOM5 and NOM6 is reported as the peak of the Gaussian mixture (main individual peak in empty circle and secondary individual peak in light grey and dashed circles) in bold, circled by an

ellipse (see Table S2), Bidirectional arrows indicate that NOM5, NOM6, NOL13 and NOL14 can be reversibly switched bidirectionally between dark and active states. **c**. Sagittal cross section diagram of the eye. The location and representative absorption range of the multiple rhodopsins expressed in each region are mapped as coloured diagonal cross patterns according to the number of rhodopsins expressed in this study and their absorption. Intra-rhabdomal filters in rows 2 and 3 of the midband row (MB) are depicted by vertical rectangles. Co, cornea; CC, crystalline cone; BM, basal membrane.

We next calculated the resulting spectral sensitivity of MB tier 2D, where NOL16, NOL17 and NOL9 (λ_{max}: 521, 537, and 541 nm, respectively) are expressed in conjunction with F1 filters (R2F1) (Fig. 3, Fig. 4a). NOL9 is present in all midband rows 1-4 [4], and presumably less likely to contribute to major differences in tier photoreceptor sensitivity. By taking into account the reported absorption spectra of R2F1 [1], our results evidence that the maximal sensitivities of NOL16 and 17 are reduced by the R2F1 filter to roughly 45% and shifted bathochromically by 16 - 18 nm (Fig. 4b,c, Extended Data Fig. 5). In addition, R2F1 narrows half bandwidth (HBW) from 100 nm to 60 - 80 nm, significantly increasing spectral discrimination in row 2 without great sensitivity loss (Extended Data Fig. 5d).

In MB tier 3D, comprising NOL9, NOL20 and NOL13, the F1 filter (R3F1) absorbs further to the red end of the visible spectrum compared to R2F1 (Fig. 4b, Extended Data Fig. 5). Therefore, in the dark, the spectral sensitivity of NOL13 and NOL20, both red shifted in absorption compared to NOL16, are still screened out by R2F1. Likewise, the resulting NOL13 and NOL20 opsin sensitivities in 3D are shifted bathochromatically by 16 nm, respectively achieving 632 nm for NOL13 and 637 nm for NOL20, on the expense of a final moderate reduction of sensitivity to 45 - 49% (Fig. 4c,e, Extended Data Fig. 5d). Since the absorption maxima of NOL16 and NOL13 are at a wavelength where transmission of the F1 filters changes the most (Extended Data

Fig. 5b), it causes compression of the HBW and shifts the sensitivity peaks of the rhodopsins with only moderate sensitivity loss (Extended Data Fig. 5c,d).

Microspectrometric data analysis in *N. oerstedii* predicted 560 nm as peak sensitivity for 3D [9], whereas electrical spectral sensitivity measurements for row 3D of two related stomatopods, *Gonodactylus smithii* and *Haptosquilla trispinosa,* placed λ_{max} at 610 nm [10]. Our calculations show that modulation of photoreceptor red light sensitivity in 3D falls above the previously proposed amplitude range for peak sensitivity with 632 nm for NOL13 and 637 nm for NOL20 in 3D (Fig. 4), demonstrating the dual role of R3F1 filtering and the multiple rhodopsin sensitivities. Reversely, we find that rhodopsins with absorption maxima near the F1 maxima are completely shielded with their sensitivity reduced over the whole spectrum accordingly. This is the case of the NOL13 photoproduct (NOL13-L, λ_{max}= 497 nm) for which sensitivity is reduced at its maximum to 7.6%, proportional to the low R3F1 filter transmission at these wavelengths (Fig. 4b,c).

In MB tiers P2 and P3, sensitivity calculations account for the reduction in light spectrum available after absorption in the distal tiers, and the high optical densities of the proximal filters (A = 7.7 for R2F2, A = 3.6 for R3F2 [1]) that further dramatically reduce the light captured by the stacked proximal tier rhodopsins. In doing so, we show that in P2, R2F2 filtering of NOL1 (λ_{max} = 540 nm) and NOL20 (λ_{max} = 607 nm) reduces their maximal sensitivities to 2.8% and 20%, respectively, and shifts the narrowed maxima to 609 nm and 641 nm (Extended Data Fig. 5d). In P3, R3F2 filtering of NOL15 shields out the rhodopsin sensitivity even further to < 0.1 % due to strongly overlapping absorbance maxima between the rhodopsin and the filter, whereas filtering of NOL20 shifts the tier

sensitivity maxima to 687 nm with a reduction to ca 2.5% (Extended Data Fig. 5). This interplay acts as the mechanism to achieve *in vivo* far-red sensitivity in row 3 in the *N. oerstedii eye.*

Trade-off photoreceptor adaptations between spectral reach and sensitivity allow vision at the far-red edge

Our findings show that the Mantis Shrimp *N. oerstedii* uses a subset of long-wavelength opsins (NOL13, 14 and 20) that absorb light maximally near or above 600 nm (Fig. 3a, Extended data Fig. 5), achieving real far-red absorbing properties by sequence modification while still coupling to the universal A1 11-*cis*-retinal chromophore. In the midband rows 2 and 3 specialized to colour vision, light of the red edge of the rhodopsin absorption spectrum can be effectively used by the employment of selective filters that absorb shorter wavelengths of light through red carotenoid pigments (Fig. 3, Extended data Fig. 5) [50,1,8,51]. This mechanism confers *N. oerstedii* with exceptional long-wavelength (far red) vision, but reduces absolute sensitivity. Hence, the magnitude of the resulting shift in effective spectral sensitivity depends on the degree of overlap between the filter's absorbance spectrum, the rhodopsin absorbance, and on the filter's optical density. High optical density and asymmetric filter-rhodopsin absorbance overlap produce large shifts (e.g. NOL1, NOL13, NOL20), whereas well-aligned opsin-filter absorption will cause a loss in photon catch and attenuate light sensitivity of the corresponding tier with little or no shift (NOL15) (Fig. 4, Extended data Fig. 5). In the proximal (P) tiers of colour-vision rows 2 and 3 (P2 and P3), the intra-rhabdomal filters are particularly optically dense, leading to substantial spectral shift reaching up to 80 nm but sacrificing sensitivity down to < 0,1%.

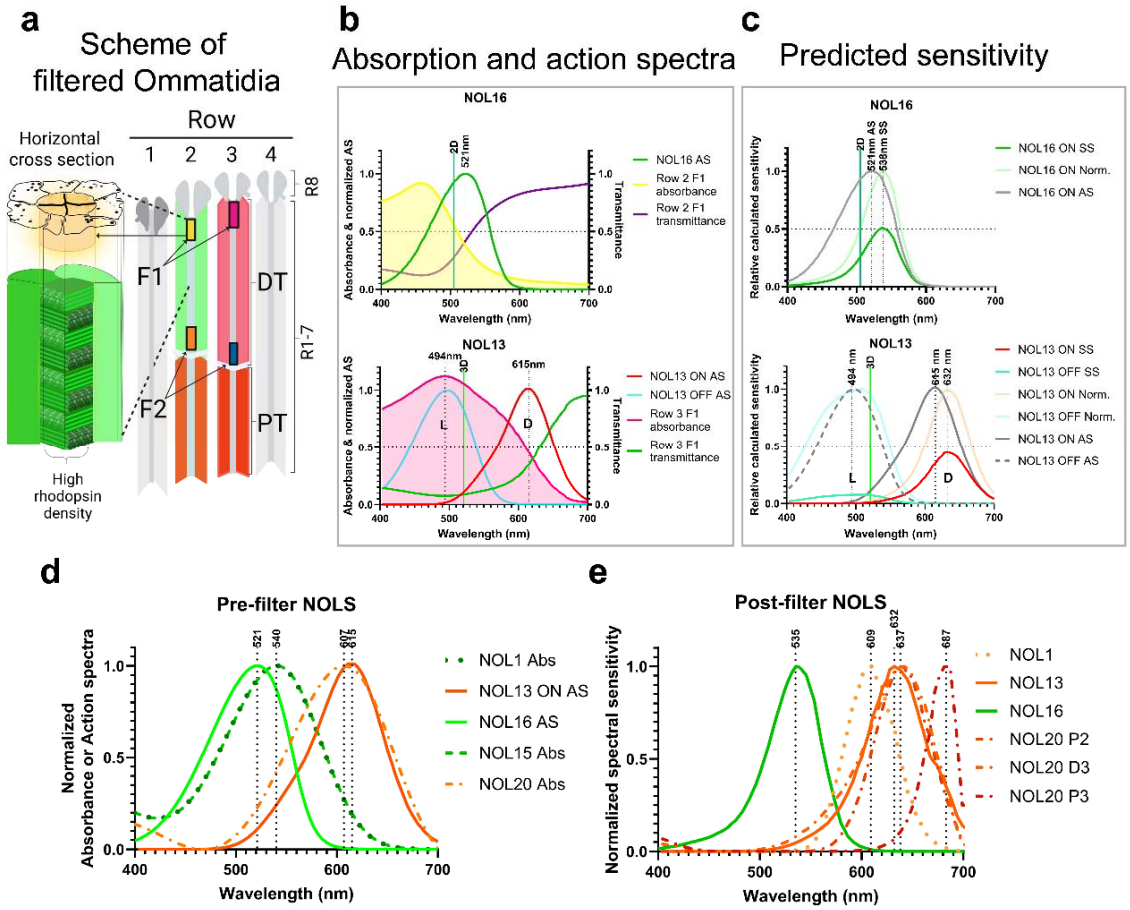

Fig. 4. Long-wavelength rhodopsins of midband rows 2 and 3 are fine tuned by intra-rhabdomal filters, extending sensitivity to the far red

a. Scheme of midband rows 2 and 3 showing the intra-rhabdomal carotenoid filters (F1 and F2) and the microvillar organisation. DT, distal tier; PT, proximal tier. Tiers in rows 2 and 3 are coloured according to the spectral sensitivity obtained with quantitative modeling of rhodopsin-filtering. **b.** Filter absorbance and transmittance [1], and wavelength absorbance of NOL16 (upper panel) and NOL13 (lower panel) of row 2 and 3 are plotted against wavelength. MSP peak absorbance of the distal tiers are indicated by the vertical line in turquoise (2D) and green (3D) [1]. L, light (ON); D, dark (OFF); AS, action spectra. See also Extended data Fig. 5. **c.** Calculated spectral sensitivity for NOL16 (upper panel) and NOL13 (lower panel) result from transmittance of the F1 filter multiplied by normalized action spectra of NOL16 and NOL13, respectively. Faint lines show the normalized sensitivities. For NOL13, activation and deactivation spectra are plotted in red and blue, respectively, and the action spectra is plotted in grey. Photoreceptor sensitivities and filtering in the UV are neglected. Half bandwidth is indicated with a bold horizontal dashed line. Norm., normalized; SS, spectral sensitivity. Sensitivities of individual additional rhodopsins are presented in Extended data Fig. 5. **d-e**. Normalized spectral sensitivities of tiers D2, P2, D3 and P3. **d.** Original rhodopsin spectra prior to i.r. filtering. **e.** Spectral sensitivity post-filtering. Maximal peak sensitivities are marked by dotted vertical lines. Post-filtering sensitivity below 0.1%, was not plotted (e.g. NOL15). AS, Action spectra; Abs, absorbance spectrum. Optical densities are reported in Extended Data Fig. 5.

Consequently, far red vision is likely restricted to bright daylight, when using P2 and P3 photoreceptors, after the distal D2 and D3 rhodopsins are already inactivated in their P-state. In contrast, at lower light levels, during dusk and dawn, colour vision relies mainly on D2 and D3 that provide a less extreme, but a more sensitive spectral range.

Overall, in *N. oerstedii*, the distal tiers of the midband ommatidia with high sensitivity are designed for low light intensities, whereas the proximal tiers are the main actors at bright light with narrowed but strongly reduced light sensitivities and a far-red maximum near 690 nm.

Mantis shrimps can therefore sample far-red wavelengths more specifically than most other animals and possess the visual capacity to potentially exploit far-red chromatic and achromatic signal reflectance (total luminance), although its contribution in an ecological context is untested behaviourally. For communication, *N. oerstedii* reliably assess total UV reflectance of competitor's meral spots [52,53], which also contribute up to 10% far red light between 700 and 800 nm [54,55]. This suggests that its eye far red sensing photoreceptors may add a signaling channel in specific ecological and visual contexts, alone or combined with UV cues or fluorescent enhancement, or at high sun angles when UV and visible spectral channels are relatively bleached and filtered out [53,56] .

Spectrally-separated rhodopsin states in the visible spectrum likely contribute to dynamic temporal signaling and colour recognition

The photoreversibility properties of at least four mantis shrimp rhodopsins are unique in the sense that they contrast to the monostable vertebrate cone rhodopsins [28], which loose the retinal after photoactivation [57–59], to the bistable invertebrate parapinopsins [60]

or *Platynereis* opsins (PdCO) [61] where one state absorbs in the visible and the other in the UV, and to the squid and jumping spider rhodopsins [62] where both D-state and L-state absorb in the visible but with strongly overlapping spectra [42,63,64].

Interestingly, in Mantis Shrimp, photoreversibility with large spectral separation of the D- and L-states without chromophore deprotonation seems to be achieved by a unique hydrogen-bonding network that fine-tunes the electronic environment and geometric distortion of the chromophore, along with large modulation upon photoisomerization, without alteration of the RSB pKa. The spectrally-separated D and L states may be an ingenious evolutionary solution to increase rapid spectral sampling between contrasting colours in natural contexts.

Collectively, the results of our current study show that the finely tuned visual system of the mantis shrimp *N. oerstedii* achieves exceptional colour discrimination notably via a diverse functional repertoire of middle and long-wavelength rhodopsins, some of which evolved photoreversibility and far-red absorption properties. Photoreversible middle and long-wavelength rhodopsin states are expected to contribute to rapid contrast perception and spectral tuning, whereas far red rhodopsins act in concert with carotenoid filtering to approach maximal sensitivity near 690 nm. Low density filters of the distal areas shift the spectra and reduce the sensitivity less and should function in dim light whereas the high density filters of the proximal tiers shift more by sacrificing sensitivity which is affordable in bright light, illustrating a series of evolutionary innovations distinct from typical animal rhodopsins, and that may carry highly beneficial adaptations in bright, spectrally broad and complex underwater environments.

Acknowledgments

The authors would like to thank Antoinette Nguyen for technical assistance, Thomas Cronin, Michael Bok, and Tillmann Utesch for stimulating discussion and Sonja Kleinlogel for discussion at a very early stage of the project. We thank Lisa Neuhold and Clint Makino (National Eye Institute) for sending us 11-*cis* retinal, Asuka Inoue for sharing the GqX plasmids, Stefan Herlitze for the HEK-GIRK1/2 cells, and Peter Soba for the HEKΔ7. The authors gratefully acknowledge the computing resources provided by the NHR Center (NHR@ZIB) through the high-performance computer "Lise" as well as by the Erlangen National High Performance Computing Center (NHR@FAU). This work was supported by the Rothschild Fellowship from Yad Hanadiv (A.P.), the Christiane Nu□sslein Volhard Stiftung (A.P), by the Hector Fellow Academy (A.M.), the European Molecular Biology Organization (EMBO) Long-Term Fellowship (ALTF 168-2021, A.P.), the Swedish Research Council (VR 2020-0517, M.A.L.), the Belgian F.R.S-FNRS (MISU F.6002.24, M.A.L.), the German Research Foundation (DFG SPP426019636, P.H.), and the European Research Council (ERC Synergy “SOL” 951644, P.H. & R.L.). P.H. is a Hertie Professor and supported by the Hertie Foundation.

Author contributions

P.H., M.A.L., M.P., A.P., C.B., and H.S. designed the experiments, M.P. provided new sequence information, C.B. expressed proteins in HEK cells, established

functional assays and recorded action spectra, A.P. did most of the molecular biology work, A.P., M.A.L., and A.M. purified protein and recorded absorption spectra. S.W. carried out QM/MM and MD simulations, R.L. and R.M. provided support for assay optimization, P.H, M.A.L., A.P. and C.B. prepared the manuscript with contributions from all authors. The authors declare no competing financial interests.

EXTENDED DATA

Extended data Figure 1. Optimisation of constructs.

Extended data Figure 2. Dark absorption and action spectra of NOL and NOM opsins.

Extended data Figure 3. G-protein selectivity profiles of NOL and NOM opsins.

Extended data Figure 4. Comparison of computed structural models between NOM6 and NOL14.

Extended data Figure 5. Effect of intra-rhabdomal filter properties on the rhodopsin spectral sensitivities in tiers D2, P2, D3 and P3.

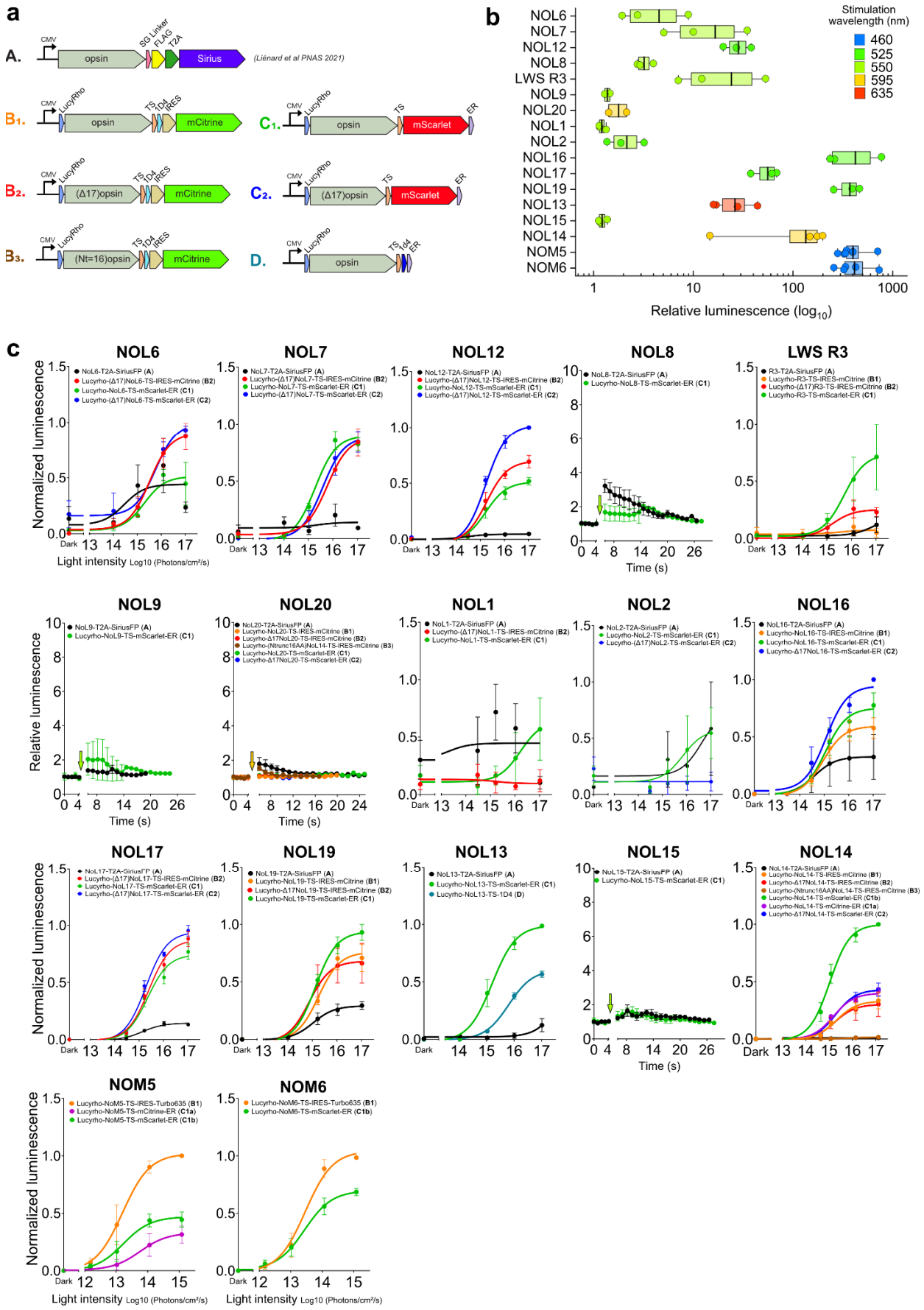
a
A.
CMV
opsin
SG Linker
FLAG
T2A
Sirius
(Liénard et al PNAS 2021)
B1.
LucyRho
TS
1D4
IRES
mCitrine
C1.
mScarlet
ER
B2.
(Δ17)opsin
C2.
B3.
(Nt=16)opsin
D.
b
NOL6
NOL7
NOL12
NOL8
LWS R3
NOL9
NOL20
NOL1
NOL2
NOL16
NOL17
NOL19
NOL13
NOL15
NOL14
NOM5
NOM6
Stimulation wavelength (nm)
460
525
550
595
635
Relative luminescence (log10)
c
Normalized luminescence
Light intensity Log10 (Photons/cm²/s)
Relative luminescence
Time (s)
Dark

Extended data Figure 1. Optimisation of constructs.

a. Design of DNA constructs used for optimisation of the luminescent responses (SG linker 2aa, 1D4 affinity tag TETSQVAPA 9aa, FLAG affinity tag DYKDDDDK 8aa, LucyRho self cleavable leucine-rich signal peptide, T2A Self cleaving peptide from *Thosea asigna* virus 2A GSGEGRGSLLTCGDVEENPGP 21aa, TS Golgi export trafficking signal sequence KSRITSEGEYIPLDQIDINV 20aa, ER endoplasmic reticulum export sequence FCYENEV 7aa, IRES internal ribosome entry site, Δ17 deletion of t17aa of an opsin N-terminus, Nt=16 only 16aa remaining upstream of TM1 of the opsin). Construct A. has been previously described [16]. **b**. Comparison of relative aequorin luminescent levels of the most effective (highest signal) constructs for each opsin following a 1s activation (wavelength indicated in the legend). **c.** Light-titration aequorin responses of various DNA constructs used in this study. Unresponsive opsins (NOL8, NOL9, NOL15, NOL20) signals are shown as relative luminescence over time, at the highest light intensity ($1x10^{17}$ photons.cm^{-2}.s^{-1}).

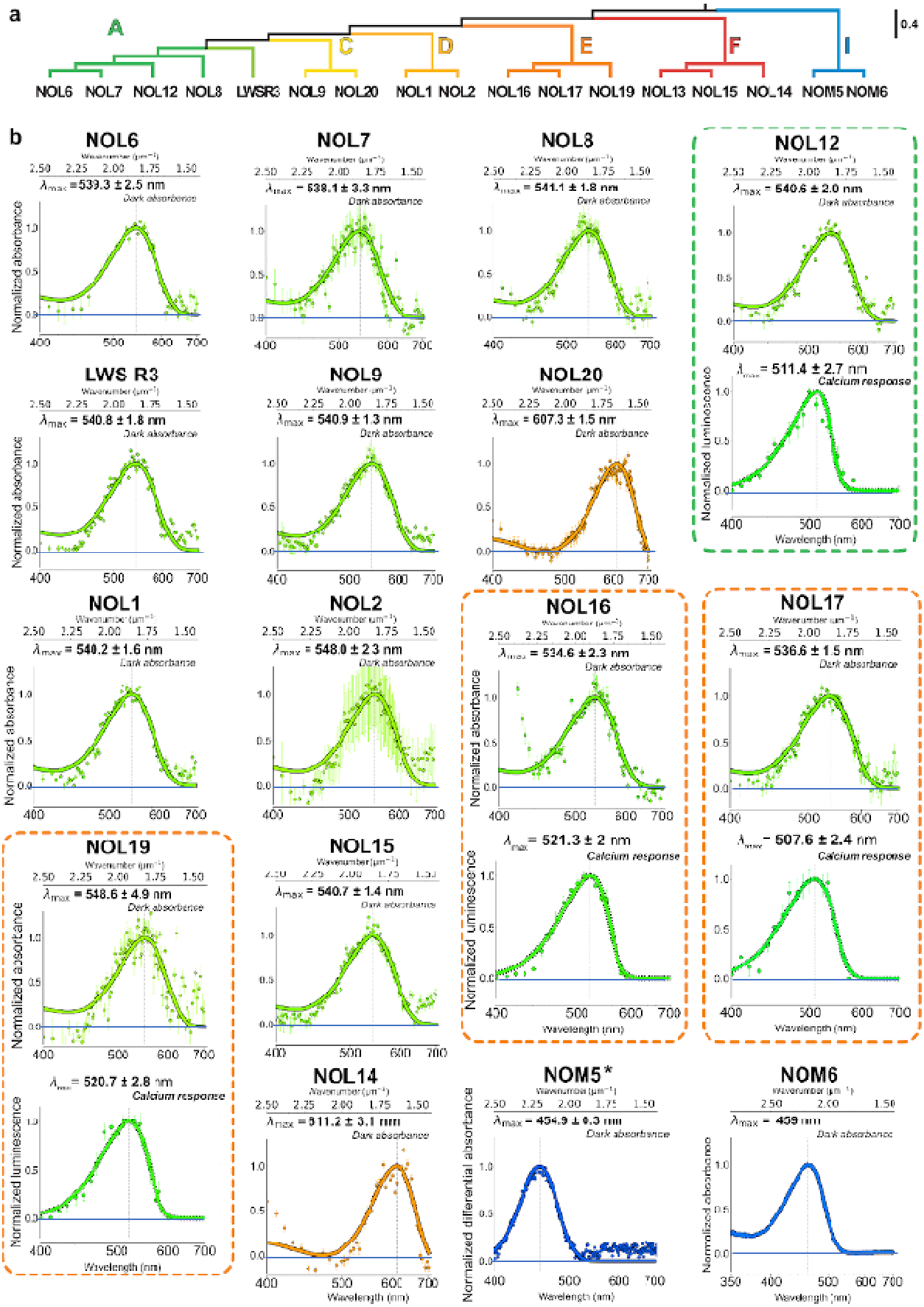
a
A
C
D
E
F
I
0.4
NOL6 NOL7 NOL12 NOL8 LWSR3 NOL9 NOL20 NOL1 NOL2 NOL16 NOL17 NOL19 NOL13 NOL15 NOL14 NOM5 NOM6
b
NOL6
λmax = 539.3 ± 2.5 nm
Dark absorbance
NOL7
λmax = 538.1 ± 3.3 nm
Dark absorbance
NOL8
λmax = 541.1 ± 1.8 nm
Dark absorbance
NOL12
λmax = 540.6 ± 2.0 nm
Dark absorbance
λmax = 511.4 ± 2.7 nm
Calcium response
LWS R3
λmax = 540.8 ± 1.8 nm
Dark absorbance
NOL9
λmax = 540.9 ± 1.3 nm
Dark absorbance
NOL20
λmax = 607.3 ± 1.5 nm
Dark absorbance
NOL1
λmax = 540.2 ± 1.6 nm
Dark absorbance
NOL2
λmax = 548.0 ± 2.3 nm
Dark absorbance
NOL16
λmax = 534.6 ± 2.3 nm
Dark absorbance
λmax = 521.3 ± 2 nm
Calcium response
NOL17
λmax = 536.6 ± 1.5 nm
Dark absorbance
λmax = 507.6 ± 2.4 nm
Calcium response
NOL19
λmax = 548.6 ± 4.9 nm
Dark absorbance
λmax = 520.7 ± 2.8 nm
Calcium response
NOL15
λmax = 540.7 ± 1.4 nm
Dark absorbance
NOL14
λmax = 511.2 ± 3.1 nm
Dark absorbance
NOM5*
λmax = 454.9 ± 4.3 nm
Dark absorbance
NOM6
λmax = 439 nm
Dark absorbance
Wavenumber (μm⁻¹)
Normalized absorbance
Normalized luminescence
Normalized differential absorbance
Wavelength (nm)

Extended data Figure 2. Dark absorption and action spectra of NOL and NOM opsins.

a. Phylogenetic relations of NOLs and NOMs from clade A, C, D, E, F and I (adapted from Porter et al. 2020).

b. Dark absorbance spectra measured in an UV-vis Nano-spectrometer after reconstitution with *11-cis* retinal, with corresponding action spectra below when possible, established from maximal aequorin responses, as indicated by the dashed frames, color coded according to phylogenetic branch. Light intensity of the 1 s pulse used for the action spectra : NOL12 : $8x10^{14}$ photons cm^{-2} s^{-1} (n=4); NOL16 (n=3) and NOL17 (n=3) : $4x10^{14}$ photons cm^{-2} s^{-1} ; NOL19 : $8x10^{13}$ photons cm^{-2} s^{-1} (n=4).

Absorbance and action spectra of all NOLs were fitted with a non-linear least squares optimization of the Govardovskii visual template to estimate the best-fit λ_{max}. Data is presented as mean values and with ±□SEM for NOLs. NOL6 and NOL14 spectra were previously reported [65]. Dark absorption for NOM5 was measured with *9-cis* retinal (*) and plotted as the differential absorbance between the dark absorption and the absorption after a 60s pulse of light (455 nm), fitted with a simple gaussian. For NOM6 a continuous spectra without any fitting but corrected for Mie scattering is shown. Bimodal action spectra for NOL13, NOL14, NOM5 and NOM6 are presented in Fig. 2.

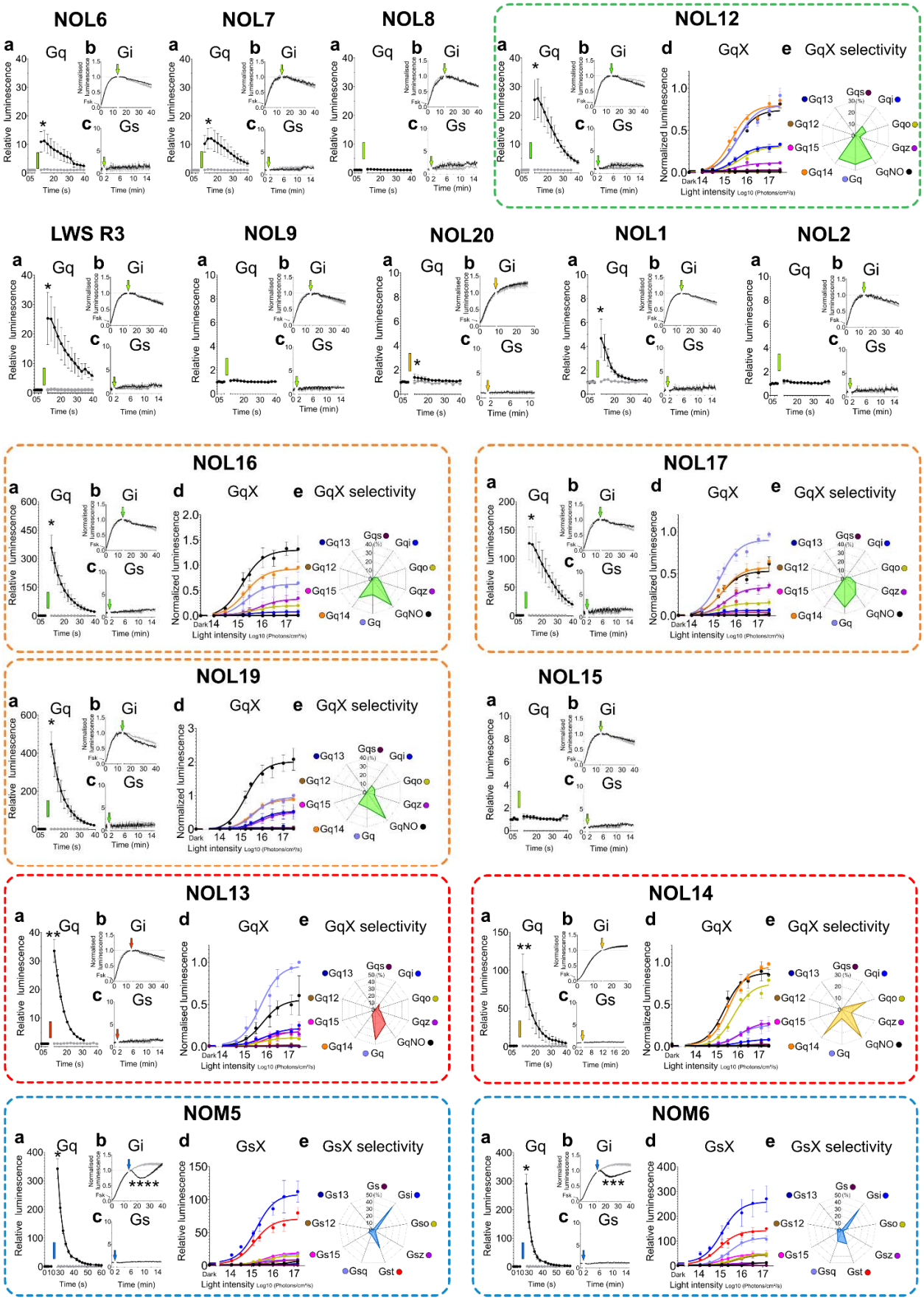
NOL6
NOL7
NOL8
NOL12
LWS R3
NOL9
NOL20
NOL1
NOL2
NOL16
NOL17
NOL19
NOL15
NOL13
NOL14
NOM5
NOM6
a Gq
b Gi
c Gs
d GqX
e GqX selectivity
d GsX
e GsX selectivity
Relative luminescence
Normalized luminescence
Time (s)
Time (min)
Light intensity Log10 (Photons/cm²/s)
Gq13
Gq12
Gq15
Gq14
Gqs
Gqi
Gqo
Gqz
GqNO
Gq
Gs13
Gs12
Gs15
Gsi
Gso
Gsz
Gsq
Gst
Gs

Extended data Figure 3. G-protein selectivity profiles of NOL and NOM opsins.

a. Responses to the Gq-protein family were measured by using the aequorin assay (see Table S1 for detailed values) **b**-**c.** Coupling efficiency to the **(b)** Gi- and **(c)** Gs-protein families in the glosensor assay. Relative luminescence values are shown as the raw luminescence divided by the averaged pre-illumination baseline. For Gi, cAMP luminescent levels were elevated using 2µM forskolin, 15 min before illumination. **d.** Light-dependent G-protein signaling was further investigated for NOMs using the GsX assay and for NOLs using the GqX assay when possible (indicated by dashed frames, colourized based on their phylogenetic clade (see Extended Data Fig. 2). Light-dependent maximal post-stimuli responses are normalized between the no GqX/GsX control and the maximal relative response **e.** Selectivity profiles were established from maximal responses to GsX or GqX chimeras and expressed as percentages of the sum of GsX or GqX protein activity.

NOL12, NOL16, NOL17, NOL19 were stimulated with 525 nm light, NOL6, NOL7, NOL8, NOL9, NOL1, NOL2, NOL15, LWS R3 with 550 nm, NOL14, NOL20 with 595 nm, and NOL13 with 635 nm. All responses were measured after a dark pre-illumination baseline followed by a 1s light pulse, indicated by colored arrows and rectangles. All data is presented as mean ± SEM. Different levels of significance at the peak are indicated by * for $p < 0.05$, ** for $p < 0.01$, *** for $p < 0.001$, and **** for $p < 0.0001$, compared to cells transfected only with luminescent reporters (grey traces).

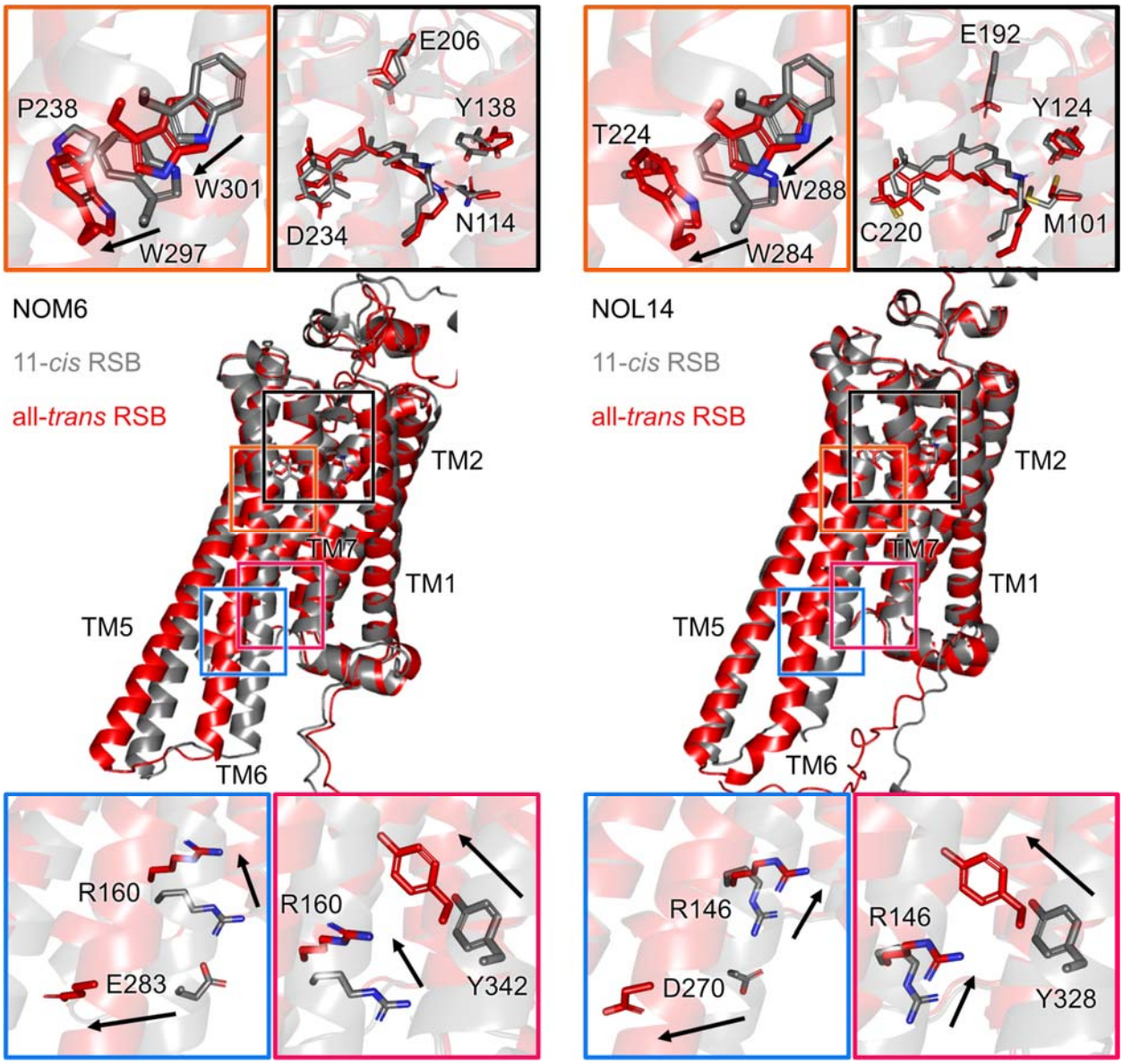

Extended data Figure 4. Comparison of computed structural models between NOM6 and NOL14. Inactive (11-*cis* retinal Schiff base bound) and active (all-*trans* retinal Schiff base bound) states are shown as gray and red cartoons, respectively. In the active states, conserved motifs undergo similar rearrangement that distinguish them from the inactive states [66]. The PIF motif contains a tryptophan substitution at position 6.44 adjacent to the CWxP tryptophan. Activation rearranges these residues (W297/W301 in NOM6 and W284/W288 in NOL14), reshaping the hydrophobic core, disrupting the DRY ionic lock (R160-E283 and R146-D270), and reorienting the NPxxY tyrosine (Y342 and Y328) toward the intracellular cavity.

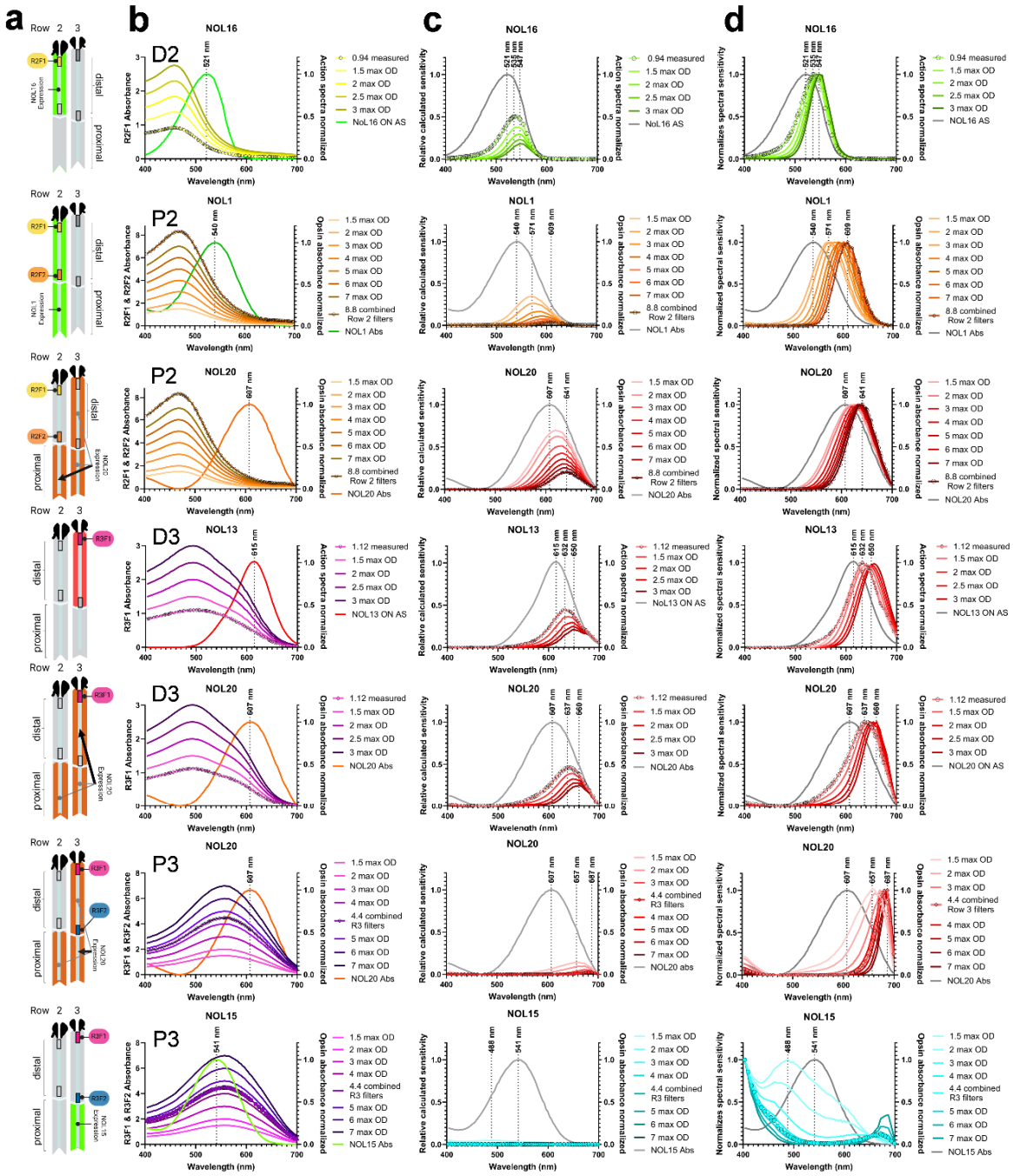

Extended data Figure 5. Effect of intra-rhabdomal filter properties on the rhodopsin spectral sensitivities in tiers D2, P2, D3 and P3.

a. Schematic representation of midband rows 2 and 3 including the rhodopsins and the filters relevant for the analysis presented in each row. **b.** Normalized rhodopsin spectra and filter spectra of different optical density ranging from 1.5 to 3 for distal (D) filters, and ranging from 1.5 to 7 for combined filters in the proximal (P) tier. Digitized filter absorbances reported in the literature [1] are labelled by black circle symbols.

c. Calculated sensitivities of the indicated rhodopsins unfiltered (grey) and after filtering by screening pigments with maximal absorbance ranging from 1.5 to 3 for distal F1 filters, and ranging from 1.5 to 7 for proximal F2 filters. Numbers above vertical dashed/dotted lines represent, from left to right, the wavelength maxima before screening, after screening by filters of reported optical densities (OD), and after maximal screening when applicable (NOL15 is almost entirely shielded by intra-rhabdomal pigments and the low resulting sensitivity could not be fitted).

d. Normalized calculated sensitivity spectra plotted with original spectral sensitivity (grey). In all graphs, absorbances and sensitivities resulting from originally measured filters [1] are labeled by black open circle symbols.

1. Cronin, T. W. & Marshall, N. J. Multiple spectral classes of photoreceptors in the retinas of gonodactyloid stomatopod crustaceans. *J. Comp. Physiol. A* **166**, 261–275 (1989).
2. Marshall, J. & Oberwinkler, J. The colourful world of the mantis shrimp. *Nature* **401**, 873–874 (1999).
3. Marshall, J., Cronin, T. W. & Kleinlogel, S. Stomatopod eye structure and function: a review. *Arthropod Struct. Dev.* **36**, 420–448 (2007).
4. Porter, M. L., Awata, H., Bok, M. J. & Cronin, T. W. Exceptional diversity of opsin expression patterns in Neogonodactylus oerstedii (Stomatopoda) retinas. *Proc. Natl. Acad. Sci.* **117**, 8948–8957 (2020).
5. Streets, A., England, H. & Marshall, J. Colour vision in stomatopod crustaceans: more questions than answers. *J. Exp. Biol.* **225**, jeb243699 (2022).
6. Cronin, T. W., Porter, M. L., Bok, M. J., Caldwell, R. L. & Marshall, J. Colour vision in stomatopod crustaceans. *Philos. Trans. R. Soc. B Biol. Sci.* **377**, 20210278 (2022).
7. Marshall, N. J., Land, M. F., King, C. A. & Cronin, T. W. The Compound Eyes of Mantis Shrimps (Crustacea, Hoplocarida, Stomatopoda). II. Colour Pigments in the Eyes of Stomatopod Crustaceans: Polychromatic Vision by Serial and Lateral Filtering. *Philos. Trans. Biol. Sci.* **334**, 57–84 (1991).

8. Cronin, T. W., Marshall, N. J., Quinn, C. A. & King, C. A. Ultraviolet photoreception in mantis shrimp. *Vision Res.* **34**, 1443–1452 (1994).

9. Cronin, T., Marshall, N. J., Caldwell, R. L. & Shashar, N. Specialization of retinal function in the compound eyes of mantis shrimps. *Vision Res.* **34**, 2639–2656 (1994).

10. Thoen, H. H., Strausfeld, N. J. & Marshall, J. Neural organization of afferent pathways from the stomatopod compound eye. *J. Comp. Neurol.* **525**, 3010–3030 (2017).

11. Wang, C.-W. J. & Marshall, N. J. Behavioural evidence of spectral opponent processing in the visual system of stomatopod crustaceans. *J. Exp. Biol.* **228**, jeb247952 (2025).

12. Cronin, T. W., Bok, M. J., Marshall, N. J. & Caldwell, R. L. Filtering and polychromatic vision in mantis shrimps: themes in visible and ultraviolet vision. *Philos. Trans. R. Soc. B Biol. Sci.* **369**, 20130032 (2014).

13. Bok, M. J., Porter, M. L. & Cronin, T. W. Ultraviolet filters in stomatopod crustaceans: diversity, ecology and evolution. *J. Exp. Biol.* **218**, 2055–2066 (2015).

14. Roberts, N. S., Hagen, J. F. D. & Johnston, R. J. The diversity of invertebrate visual opsins spanning Protostomia, Deuterostomia, and Cnidaria. *Dev. Biol.* **492**, 187–199 (2022).

15. Cronin, T. W., Johnsen, S., Marshall, J. & Warrant, E. J. *Visual Ecology*. (Princeton University Press, 2014).

16. Liénard, M. A. *et al.* The evolution of red color vision is linked to coordinated rhodopsin tuning in lycaenid butterflies. *Proc. Natl. Acad. Sci.* **118**, e2008986118 (2021).

17. Merbs, S. L. & Nathans, J. Absorption spectra of human cone pigments. *Nature* **356**, 433–435 (1992).

18. Parry, J. W. L. *et al.* Mix and Match Color Vision: Tuning Spectral Sensitivity by Differential Opsin Gene Expression in Lake Malawi Cichlids. *Curr. Biol.* **15**, 1734–1739 (2005).

19. Sharkey, C. R., Blanco, J., Lord, N. P. & Wardill, T. J. Jewel Beetle Opsin Duplication and Divergence Is the Mechanism for Diverse Spectral Sensitivities. *Mol. Biol. Evol.* **40**, msad023 (2023).

20. Spady, T. C. *et al.* Evolution of the Cichlid Visual Palette through Ontogenetic Subfunctionalization of the Opsin Gene Arrays. *Mol. Biol. Evol.* **23**, 1538–1547 (2006).

21. Yokoyama, S. Molecular evolution of vertebrate visual pigments. *Prog. Retin. Eye Res.* **19**, 385–419 (2000).

22. Corbo, J. C. Vitamin A1/A2 chromophore exchange: Its role in spectral tuning and visual plasticity. *Dev. Biol.* **475**, 145–155 (2021).

23. Corredor, V. H., Hauzman, E., Gonçalves, A. da S. & Ventura, D. F. Genetic characterization of the visual pigments of the red-eared turtle (Trachemys scripta elegans) and computational predictions of the spectral sensitivity. *J. Photochem. Photobiol.* **12**, 100141 (2022).

24. Enright, J. M. *et al.* Cyp27c1 Red-Shifts the Spectral Sensitivity of Photoreceptors by Converting Vitamin A1 into A2. *Curr. Biol.* **25**, 3048–3057 (2015).

25. Escobar-Camacho, D. *et al.* Variable vision in variable environments: the visual system of an invasive cichlid (Cichla monoculus) in Lake Gatun, Panama. *J. Exp. Biol.* **222**, jeb188300 (2019).

26. Loew, E. R. & Govardovskii, V. I. Photoreceptors and visual pigments in the red-eared turtle, Trachemys scripta elegans. *Vis. Neurosci.* **18**, 753–757 (2001).

27. Partridge, J. C. & Douglas, R. H. Far-red sensitivity of dragon fish. *Nature* **375**, 21–22 (1995).

28. Imamoto, Y. & Shichida, Y. Cone visual pigments. *Biochim. Biophys. Acta BBA - Bioenerg.* **1837**, 664–673 (2014).

29. Kooi, C. J. van der, Stavenga, D. G., Arikawa, K., Belušič, G. & Kelber, A. Evolution of Insect Color Vision: From Spectral Sensitivity to Visual Ecology. *Annu. Rev. Entomol.* **66**, 435–461 (2021).

30. Donohue, M. W., Carleton, K. L. & Cronin, T. W. Opsin Expression in the Central Nervous System of the Mantis Shrimp Neogonodactylus oerstedii. *Biol. Bull.* **233**, 58–69 (2017).

31. Gleadall, I. G., Hariyama, T. & Tsukahara, Y. The visual pigment chromophores in the retina of insect compound eyes, with special reference to the Coleoptera. *J. Insect Physiol.* **35**, 787–795 (1989).

32. Goldsmith, T. H. & Cronin, T. W. The retinoids of seven species of mantis shrimp. *Vis. Neurosci.* **10**, 915–920 (1993).

33. Suzuki, T. & Eguchi, E. A survey of 3-dehydroretinal as a visual pigment chromophore in various species of crayfish and other freshwater crustaceans. *Experientia* **43**, 1111–1113 (1987).

34. Cronin, T. W., Marshall, N. J. & Caldwell, R. L. Visual pigment diversity in two genera of mantis shrimps implies rapid evolution (Crustacea; Stomatopoda). *J. Comp. Physiol. A* **179**, 371–384 (1996).

35. Helena J. Bailes, R. J. L. Human melanopsin forms a pigment maximally sensitive to blue light (λmax ≈ 479 nm) supporting activation of Gq/11 and Gi/o signalling cascades | Proceedings of the Royal Society B: Biological Sciences. *Proc. R. Soc. B.* https://doi.org/10.1098/rspb.2012.2987 (2013) doi:10.1098/rspb.2012.2987.

36. Inoue, A. *et al.* Illuminating G-Protein-Coupling Selectivity of GPCRs. *Cell* **177**, 1933-1947.e25 (2019).

37. Ballister, E. R., Rodgers, J., Martial, F. & Lucas, R. J. A live cell assay of GPCR coupling allows identification of optogenetic tools for controlling Go and Gi signaling. *BMC Biol.* **16**, 10 (2018).

38. Inoue, A. *et al.* TGFα shedding assay: an accurate and versatile method for detecting GPCR activation. *Nat. Methods* **9**, 1021–1029 (2012).

39. McDowell, R. J. *et al.* Beyond Lux: methods for species and photoreceptor-specific quantification of ambient light for mammals. *BMC Biol.* **22**, 257 (2024).

40. Foster, K. W. Chapter 3 Action spectroscopy of photomovement. in *Comprehensive Series in Photosciences* (eds Häder, D.-P. & Breure, A. M.) vol. 1 51–115 (Elsevier, 2001).

41. Foster, R. G. & Hankins, M. W. Circadian vision. *Curr. Biol. CB* **17**, R746-751 (2007).

42. Koyanagi, M. *et al.* High-performance optical control of GPCR signaling by bistable animal opsins MosOpn3 and LamPP in a molecular property–dependent manner. *Proc. Natl. Acad. Sci.* **119**, e2204341119 (2022).

43. Wagdi, A. *et al.* Selective optogenetic control of Gq signaling using human Neuropsin. *Nat. Commun.* **13**, 1765 (2022).

44. Bailes, H. J., Zhuang, L.-Y. & Lucas, R. J. Reproducible and Sustained Regulation of Gαs Signalling Using a Metazoan Opsin as an Optogenetic Tool. *PLOS ONE* **7**, e30774 (2012).

45. Abramson, J. *et al.* Accurate structure prediction of biomolecular interactions with AlphaFold 3. *Nature* **630**, 493–500 (2024).

46. Stein, R. A. & Mchaourab, H. S. SPEACH_AF: Sampling protein ensembles and conformational heterogeneity with Alphafold2. *PLOS Comput. Biol.* **18**, e1010483 (2022).

47. Honig, B. *et al.* An external point-charge model for wavelength regulation in visual pigments. *J. Am. Chem. Soc.* **101**, 7084–7086 (1979).

48. Nakanishi, K., Balogh-Nair, V., Arnaboldi, M., Tsujimoto, K. & Honig, B. An external point-charge model for bacteriorhodopsin to account for its purple color. *J. Am. Chem. Soc.* **102**, 7945–7947 (1980).

49. Warrant, E. J. & Johnsen, S. Vision and the light environment. *Curr. Biol.* **23**, R990–R994 (2013).

50. Bernard, G. D. Red-Absorbing Visual Pigment of Butterflies. *Science* **203**, 1125–1127 (1979).

51. Lamb, T. D. Photoreceptor spectral sensitivities: common shape in the long-wavelength region. *Vision Res.* **35**, 3083–3091 (1995).

52. Chiou, T.-H., Place, A. R., Caldwell, R. L., Marshall, N. J. & Cronin, T. W. A novel function for a carotenoid: astaxanthin used as a polarizer for visual signalling in a mantis shrimp. *J. Exp. Biol.* **215**, 584–589 (2012).

53. Mazel, C. H., Cronin, T. W., Caldwell, R. L. & Marshall, N. J. Fluorescent Enhancement of Signaling in a Mantis Shrimp. *Science* **303**, 51–51 (2004).

54. Franklin, A. M., Applegate, M. B., Lewis, S. M. & Omenetto, F. G. Stomatopods detect and assess achromatic cues in contests. *Behav. Ecol.* **28**, 1329–1336 (2017).

55. Franklin, A. M. *et al.* Differences in signal contrast and camouflage among different colour variations of a stomatopod crustacean, Neogonodactylus oerstedii. *Sci. Rep.* **10**, 1236 (2020).

56. Donohue, M. W., Cohen, J. H. & Cronin, T. W. Cerebral photoreception in mantis shrimp. *Sci. Rep.* **8**, 9689 (2018).

57. Rando, R. R. Molecular mechanisms in visual pigment regeneration. *Photochem. Photobiol.* **56**, 1145–1156 (1992).

58. Morshedian, A. *et al.* Light-Driven Regeneration of Cone Visual Pigments through a Mechanism Involving RGR Opsin in Müller Glial Cells. *Neuron* **102**, 1172-1183.e5 (2019).

59. Sakai, K., Shichida, Y., Imamoto, Y. & Yamashita, T. Creation of photocyclic vertebrate rhodopsin by single amino acid substitution. *eLife* **11**, e75979 (2022).

60. Koyanagi, M. *et al.* Diversification of non-visual photopigment parapinopsin in spectral sensitivity for diverse pineal functions. *BMC Biol.* **13**, 73 (2015).

61. Wietek, J. *et al.* A bistable inhibitory optoGPCR for multiplexed optogenetic control of neural circuits. *Nat. Methods* **21**, 1275–1287 (2024).

62. Nagata, T. *et al.* The counterion–retinylidene Schiff base interaction of an invertebrate rhodopsin rearranges upon light activation. *Commun. Biol.* **2**, 180 (2019).

63. Rodrigues, M. J. *et al.* Activating an invertebrate bistable opsin with the all-trans 6.11 retinal analog. *Proc. Natl. Acad. Sci.* **121**, e2406814121 (2024).

64. Terakita, A., Hara, R. & Hara, T. Retinal-binding protein as a shuttle for retinal in the rhodopsin-retinochrome system of the squid visual cells. *Vision Res.* **29**, 639–652 (1989).

65. Liénard, M. A., Valencia-Montoya, W. A. & Pierce, N. E. Molecular advances to study the function, evolution and spectral tuning of arthropod visual opsins. *Philos. Trans. R. Soc. B Biol. Sci.* https://doi.org/10.1098/rstb.2021.0279 (2022) doi:10.1098/rstb.2021.0279.

66. Zhou, Q. *et al.* Common activation mechanism of class A GPCRs. *eLife* **8**, e50279 (2019).